



Adaptive Thermoforming and Structural Design of Millimeter-Wave Antenna Panels

Zack Hatfield¹ · Alex St. Peter¹ · Christian Davila-Peralta² · Joel Berkson¹ · Daewook Kim^{1,2} · Justin Hyatt²

Received: 9 July 2022 / Revised: 19 September 2022 / Accepted: 22 September 2022
© The Author(s) 2022

Abstract

Future large-scale radio telescope observatories, such as the next-generation Very Large Array, involve extremely large collection areas. These collection areas are divided into smaller shaped panels, which typically require their own unique molds to manufacture. For these projects to be cost-effective, an efficient fabrication method for the shaped panels is needed. This paper outlines the development and success of a novel adaptive freeform panel molding technology that greatly improves manufacturing efficiency due to its repeatable and reusable nature. Moreover, it presents an analysis of a proposed panel structural design for the shaped panels, which incorporates a study on surface deformation due to gravity and wind loading under realistic operational conditions.

Keywords Radio telescope · Millimeter-wave · Thermoform · Adaptable mold

1 Introduction

Radio astronomy is a subdivision within the field of astronomy that dates back nearly 90 years. It is specifically focused on studying the cosmos through telescopes designed to operate in the radio wavelength range. The radio wavelength range is the portion of the electromagnetic spectrum ranging from roughly 1 mm to 1000 km or 1 THz to 10 kHz in frequency [1]. “Millimeter wave” refers to the range of frequencies within the broader radio spectrum that corresponds to wavelengths on the scale of millimeters.

In general, high sensitivity, angular resolution, dynamic range, and spectrum coverage are all desirable, with trade-offs made in the telescope or communication antenna design process to optimize the balance of these traits for the scientific or technical requirements of the system. As a result of

the poor angular resolution due to diffraction, the primary reflector of a radio telescope or antenna tends to be significantly larger than that of the largest optical telescopes, with aperture diameters of over 10 m commonplace [2]. As an example, a 13-m aperture communication antenna dish manufactured using a thermoforming technique is shown in Fig. 1.

The required surface figure root mean square (RMS) error of the primary reflector surface when compared to its desired shape is in the 10 s of microns for the millimeter-wave operation [3]. Specifically, according to the antenna tolerance theory, telescopes with the shortest operational wavelength of 1 mm require a reflector surface RMS error smaller than 60 μm for optimal performance [4]. To achieve these surface figure error and primary mirror diameter requirements, reflectors are typically made from multiple aluminum panels. These aluminum panels are individually shaped to be patterned together to approximate the full reflector surface. Oftentimes, this surface is either parabolic or hyperbolic due to the typical Cassegrain-style design of most shorter-wavelength radio and millimeter-wave telescopes [1].

Historically, four main manufacturing techniques have been used to fabricate panels used for several prominent radio and millimeter-wavelength telescopes, each with its own advantages and disadvantages. These include the techniques of machining, stretching, electroforming, and using carbon fiber-reinforced plastic. Although each of these

✉ Daewook Kim
dkim@optics.arizona.edu

✉ Justin Hyatt
justinhj@email.arizona.edu

¹ James C. Wyant College of Optical Sciences, University of Arizona, 1630 E. University Blvd, Tucson, AZ 85721, USA

² Department of Astronomy and Steward Observatory, University of Arizona, 933 N. Cherry Ave, Tucson, AZ 85721, USA



Fig. 1 Segmented 13-m-diameter communication antenna dish with 60 thermoformed precision panels

techniques can achieve surface figure RMS error values within the range of typical telescope requirements, they have downsides related to their cost, fabrication lead time, and efficiency for varied panel geometries. Specifically, machining panels individually requires an extremely large investment in time and money. However, these repetitive and complicated manufacturing processes have been necessary for many radio telescope systems due to the numerous and varied panel shapes required for large dishes. Alternatively, the electroforming, carbon fiber-reinforced plastic, and stretching methods all require a unique mold that matches the desired surface shape of the panel for use in their respective manufacturing processes [4, 5]. This process results in high material costs and time expended on machines or otherwise generates custom molds for each unique panel.

As the demand for a high volume of radio and millimeter-wave telescopes grows with large-scale projects, such as the next-generation Very Large Array (ngVLA), drawing closer, more efficient, adaptable, and cost-effective panel fabrication processes has become increasingly more important to support the growing science and engineering communities. In an effort to address these demands and improve panel manufacturing efficiency, a significant research effort has been poured into the development of a robust and efficient method of adaptive aluminum thermoforming for the fabrication of radio and millimeter-wave telescope panels to assist the evolving radio telescope industry. This method's foundation relies on an adaptive mold, which can change its surface shape to approximate a range of different freeform curvatures. This method allows for a single mold that could be used to fabricate all the panels for an entire millimeter- or radio-wave telescope dish. In addition, by providing a

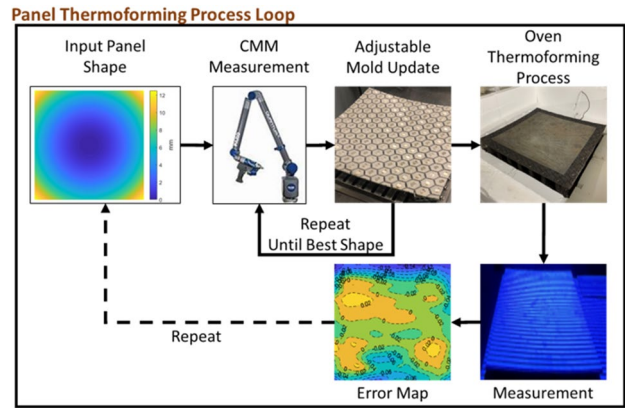


Fig. 2 Current adaptable mold thermoforming process loop, showing the flow of its iterative steps

platform for a detailed investigation into the phenomena, an adaptable mold has the potential to address the springback challenge associated with the heating and cooling involved in shaping aluminum to specific curvatures. In the following sections, we will present the details of this method while primarily focusing on the research and development of the adaptable mold technology.

2 Adaptive Thermoforming

The adaptive aluminum thermoforming process involves placing flat aluminum sheets on an adjustable freeform mold designed to approximate a particular surface shape designated for the panel and then heating up the whole setup in an oven until the panel exceeds its elastic limit and conforms to the mold. The overall thermoforming process flow is depicted in Fig. 2.

The adaptable thermoforming procedure began by placing the adaptable mold in the center of the oven, centering the panel on top of the mold surface, and loading the top of the panel with a uniform and heavy weight. This weight consisted of a 50 lb. steel chain, coiled up to semi-evenly distribute the load across the panel surface. This process ensures that the panel conforms to the shape of the mold upon heating. The lid of the oven was closed, and the temperature was controlled to heat at a linear rate until it reached 600 °C. Two wire thermocouples were used to monitor the temperature in the oven, with one set up to allow for the estimation of the mold temperature and the other one to read the temperature of the air above the mold. Once the temperature of the mold reached 600 °C, the oven was controlled to maintain this temperature for approximately 1 h. Then, it was turned off entirely and left to cool at its own natural rate. Typically, it took nearly 3–4 h for the oven to reach the temperature and another 7–8 h to cool back to room temperature. Once

cooled, the panel was removed from the oven and measured. In high volume production, using a tunnel kiln would greatly decrease the per-part time.

For the panel shape measurement, we used a metrology method developed in our lab based on concepts from stereophotogrammetry and fringe projection profilometry, whose layout is shown below [6]. The method utilizes two cameras calibrated using MATLAB's Stereo Camera Calibrator App and a gaming projector. Rather than physically placed fiducial markers, as typically done in photogrammetric metrology, a projector was used to create fiducials via phase encoding. Two sets of phase-shifted sinusoidal patterns were used, encoding every point on the panel with a unique phase pair, which is used for feature matching between the two cameras.

Using the two cameras' calibrated parameters and the set of matched features, a point cloud representing the surface figure was produced via triangulation, as depicted in Fig. 3. This method has been demonstrated to produce surface accuracies better than 10 μm RMS over a square meter. This method also produces extremely dense spatial sampling on the panel surface (millions of points per square meter), which allows for a more in-depth investigation into the causes and effects of our adaptive thermoforming panel manufacturing techniques.

In Sects. 3 and 4, we describe the performance of the full thermoforming process loop, focusing specifically on the shaping capabilities of the adjustable mold and resulting precision-shaped panels, respectively. However, the testing associated with these results was accomplished with a coordinate measuring machine (CMM) because the fringe projection metrology system was still in development at the time of those experiments.

One of the main technical challenges associated with the thermoforming process is the springback phenomenon, which describes the tendency for aluminum to relax back toward its original pre-thermoformed shape by some non-trivial amount upon cooling, creating a significant surface figure error [7]. This problem is an especially difficult one to deal with in the context of millimeter-wave telescope panels

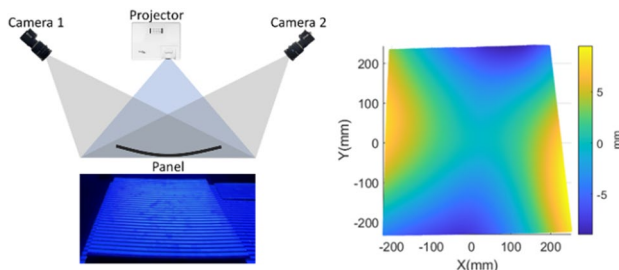


Fig. 3 Stereo fringe projection profilometry layout (top left), sample image of the projected pattern (bottom left), and resulting surface measurement (right)

due to the relatively tight surface figure quality requirements. By developing an adaptable mold that can change its surface shape to approximate a range of different freeform curvatures, a single mold could be used to fabricate panels for an entire millimeter- or radio-wave telescope dish. This approach can greatly reduce panel fabrication costs and improve manufacturing efficiency for the radio telescope industry. Moreover, an adaptable mold can address the springback challenge by iteratively forming panels and compensating for the springback by adjusting the mold shape.

The magnitude of the springback effect depends on many variables, likely including the surface area, panel thickness, and concavity of the panel. An adaptable mold allows for these variables to be investigated by performing tests involving the adjustment of the surface to approximate various shapes, thermoforming panels on the mold, and comparing the panel shape to the mold shape. This investigation facilitates the development of a predictive model to describe the springback as a function of relevant panel parameters and could result in a fabrication procedure that involves setting the mold to a “pre-corrected” surface shape, yielding a thermoformed panel closely approximating the desired shape upon cooling. In Sects. 3 and 4, we summarize our outcome demonstrating these ideas.

3 Adaptable Mold Design and Development

The driving technology presented is an adaptable mold used to thermoform panels with varying compound freeform curvatures [8]. This mold consists of several components that have been designed, constructed, and tested. The first main feature is a flexible steel sheet that can be described as a patterning of individual tiles, each connected to its neighbors via thin flexures. The second feature is an array of actuators connected to some of the tiles, which are controlled to move independently of one another in the vertical direction. By adjusting these tiles in the piston, their centers can be set at the desired height, which will vary their slopes, allowing for different curvatures to be approximated by the entire mold surface. The heights of each of the tiles are precisely controlled by adjusting actuator bolts, and the distance that each bolt travels is directly dependent on the bolt rotation and thread pitch. A view of the fully assembled adaptable mold is shown in Fig. 4 (right), where the whole structure can be seen. A two-dimensional drawing of these features in a basic format in Fig. 4 (left) demonstrates how they work together to create an adjustable mold that can be used to approximate different surface curvatures [5].

As the primary application for this mold is to fabricate millimeter-wave telescope panels, we set the mold shape to a paraboloidal section with a focal length of 2.5 m. To set the mold shape, we developed an iterative process that involved

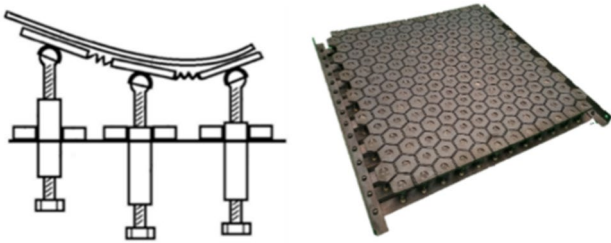


Fig. 4 (Left) Adaptable mold concept drawing. (right) Orthogonal view of the fully assembled adaptable mold

measuring the mold surface with a CMM, fitting the point cloud data to the paraboloidal surface equation, and then calculating the residual error as exemplified in Fig. 5.

The residual error for each data point was used to generate an array of vertical distance values for each tile that would bring them to the location that satisfied the fit. These distance values were then transformed into the required degrees of rotation for each bolt actuator, and the adjustment process could proceed by rotating every bolt the specified amount. Once this process was completed, the mold surface was measured again, and the process was repeated through multiple iterations until the RMS error of the fit could no longer significantly decrease over the span of several iteration cycles. The RMS error value of the measured data compared with the paraboloidal fit was therefore used as the primary metric for judging the shaping capabilities of the mold, and this value was recorded for each iteration. In Fig. 5, the RMS error vs. iteration number is plotted in a bar graph format. The lowest RMS error achieved was 54 microns.

4 Adaptive Thermoforming Performance

Over the course of our experimentation with the adaptable mold, we successfully thermoformed several panels to a precisely prescribed shape after performing adjustment iterations, as shown in Fig. 6.

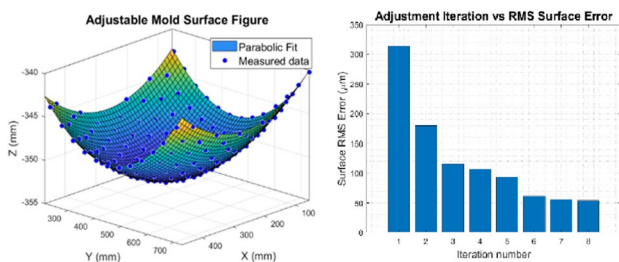


Fig. 5 (Left) Portable CMM point cloud data and paraboloidal surface fit for the adaptable mold. (right) Adjustment iteration number vs. surface figure RMS error for the shaped adaptable mold

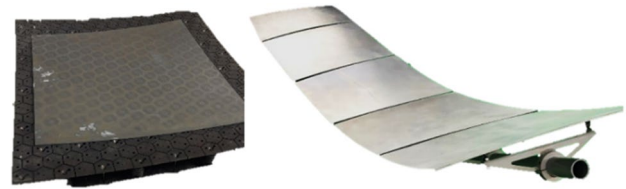


Fig. 6 (Left) Thermoformed panel resting on the adaptable mold. (right) Multiple thermoformed panels mounted together to collectively construct a freeform shape

For one particular experiment, the target shape was a paraboloid with a 5-m radius of curvature. Three 500 mm × 500 mm flat pieces of aluminum were thermoformed on the mold. These panels were all measured using the same CMM that was used to measure the mold during adjustment iterations (the fringe projection metrology technique described in Sect. 2 was still in development at this time). The results are summarized in Table 1, showing the best fit paraboloid surface equation parameters, focal length, and RMS error values.

The results successfully demonstrate that the three different thermoformed panels each achieved similar paraboloidal shapes with similar RMS errors of less than 100 microns, which can operate for very short wavelength applications, such as ~2 mm. All three panels have best fits to paraboloids with focal lengths longer than the paraboloid that the adaptable mold was shaped to. This effect is an example of the springback phenomena that was described in Sect. 2 and can be calibrated out through an iterative process if necessary. To further understand these results, the best fit focal length for each panel was averaged to define a mean focal length with the standard deviation. The mean focal length is $-2,879.8 \text{ mm} \pm 34.5 \text{ mm}$ (standard deviation $\pm \sigma$). Using the mean focal length, an associated equation for the paraboloid that best characterizes all three of the panels can be defined. All three panels were fitted to the surface to estimate the repeatability of the springback effect on the panels and the thermoforming process itself. The results are displayed in Table 2.

The mean best fit focal length of all three panels was approximately 380 mm longer compared to the mold shape at the time of thermoforming. This result implies that the springback effect increased the best fit radius of curvature of the panels in comparison to the best fit mold shape by a factor of 1.15, which is the calibration factor. In addition, the repeatability of this phenomenon was consistent, resulting in panels of the same shape with an RMS error difference between panels in the range of 3 microns. Finally, the overall surface fit of the panels to the mean focal length equation increased in the RMS error by a consistent value of around 35 microns compared to the RMS error value fit to the mold shape. The springback effect not only changed

Table 1 Thermoformed panel accuracy (best fit focal length)

Fit characteristics	Panel 1	Panel 2	Panel 3
Equation parameters $f(x, y) = a \cdot (x^2 + y^2) + b \cdot x + c \cdot y + d$ (mm)	$a = -8.577 \times 10^{-5}$ $b = 0.04093$ $c = 0.06863$ $d = -215.7$	$a = -8.684 \times 10^{-5}$ $b = 0.04133$ $c = 0.06971$ $d = -216$	$a = -8.785 \times 10^{-5}$ $b = 0.07218$ $c = 0.07481$ $d = -434.7$
Focal length (mm)	-2,914.8	-2,878.9	-2,845.8
Residual RMS error (μm)	85.32	88.32	88.19

Table 2 Thermoformed panel accuracy (mean focal length)

Fit characteristics	Panel 1	Panel 2	Panel 3
Equation parameters $f(x, y) = a \cdot (x^2 + y^2) + b \cdot x + c \cdot y + d$ (mm)	$a = -8.6812 \times 10^{-5}$ $b = 0.0414$ $c = 0.06948$ $d = -215.9$	$a = -8.6812 \times 10^{-5}$ $b = 0.04132$ $c = 0.06969$ $d = -216$	$a = -8.6812 \times 10^{-5}$ $b = 0.07133$ $c = 0.07393$ $d = -434.4$
Focal length (mm)	-2,879.8	-2,879.8	-2,879.8
Residual RMS error (μm)	89.51	88.1	91.64

the panel surface shape by a repeatable ratio but also consistently increased the RMS surface figure error of this shape in comparison to the mold shape.

5 Reflector Panel Structural Design

In addition to the development of a novel adaptive panel molding technology, we also researched a structural panel design that could be considered for application toward panels fabricated in the full thermoforming process loop. This was performed to create a more complete, end-to-end panel fabrication demonstration and provide a proof of concept for applying our technology to real-world engineering applications.

Two panel designs were analyzed. The first option uses two thermoformed plates glued to an aluminum honeycomb core in a sandwich fashion, similar to what is performed in the electroforming panel fabrication. Although it had good results with the prototype fabrication, this option was discarded because it requires two thermoformed panels, which causes potential cost increases. The second option uses one aluminum 5052, 3.175-mm-thick plate thermoformed, with slotted ribs glued on its back, as shown in Fig. 7. The panel parameters are presented in Table 3.

An important feature of the reflector panel is the method in which it is mounted to the support structure, as overconstraining can have a negative impact on the panel performance, especially during thermal cycles with thermally induced deformations and panel installation and pointing. Other specifications include that adjusters must maintain their position under operating conditions and meet various survival conditions. The adjusters should also attach to the panel at its neutral plane.

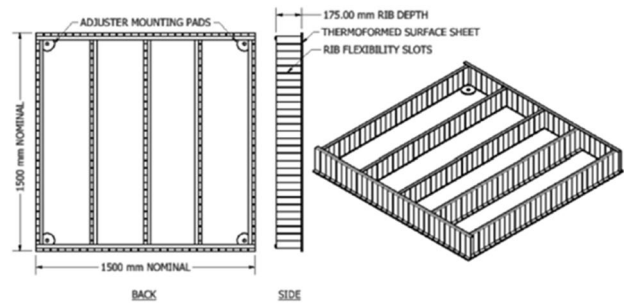


Fig. 7 Reference panel design for the ngVLA primary reflector used as the baseline for our final structural panel design

Table 3 Proposed panel parameters

Panel characteristics	Value
Reflector dimensions	1.5 m × 1.5 m
Skin thickness	3.175 mm
Material	Al 5052
Weight	40.112 kg
Pads	1 rigid, 3 flexible (2 DoF)
Rib height	175 mm

The team came up with an adjuster solution inspired by the one used by the Atacama Large Millimeter/submillimeter Array telescope, consisting of a double-screw mechanism that can be precisely adjusted while facing the front/reflective side of the panel. An analytical calculation determined the required resolution of precision of the adjusters. The

team calculated the RMS surface error caused by a unit shift of the panel adjusters:

$$RMSE_{\text{panel}} = \frac{\text{Error}_{\text{adjuster}}}{\sqrt{3}}, \tag{1}$$

where $RMSE_{\text{panel}}$ is the RMS surface error of the panel and $\text{Error}_{\text{adjuster}}$ is the error associated with the adjuster mechanism precision. As an example, if a panel adjuster is 10 μm away from its correct position, the resulting misalignment will cause 6 μm of shape error to the panel surface. Based on this, an adjuster precision of 1 micron per degree of tool rotation is required to achieve a 100 μm RMS surface error over the reflector surface. For the proposed panel, one adjuster was set fixed to the structure, while the others had 2 degrees of freedom (DoF) on the plane parallel to the reflector (i.e., x and y , and z is normal to the reflector face) to allow for thermal expansion. These DoFs were obtained using a leveling washer. The proposed adjuster can be installed and adjusted using standard metric tools. The adjuster had a precision of 0.7 microns per degree of tool rotation. The adjuster had an axial thermal expansion coefficient of $17.8 \times 10^{-6}/\text{K}$.

6 Operational Performance of the Panel Structural Design

To confirm the panel structural design’s effectiveness and performance in real-world applications, a detailed analysis aided by a finite element analysis (FEA) simulation was performed to characterize the deformation of the panel due to gravity and wind loading effects for several different operational conditions.

The coefficients for calculating the wind drag on antenna panels were taken from the McAuliffe report [9], where the same coordinate system convention was also

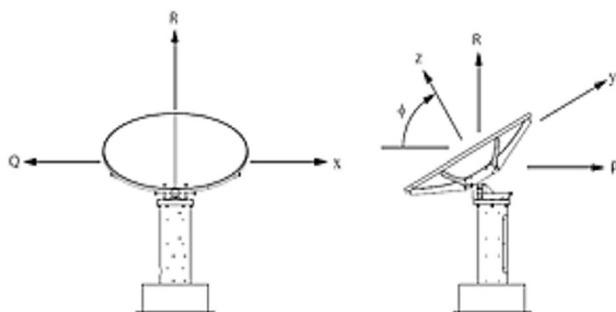


Fig. 8 Coordinate system convention according to the McAuliffe report of the wind tunnel simulation for the Square Kilometer Array [9]

used to facilitate the load identification shown in Fig. 8. To facilitate the calculations of the concept study, a single central panel with a central normal vector that is parallel and opposite to the wind direction was considered for the calculations.

The most critical orientation for the telescope is at azimuth = 0 deg and elevation = 30 deg, as it presents the largest drag coefficient. The wind drag for the laminar wind flow was approximately $C_{FP} = 1.2$, as shown in Fig. 9, which is the same coefficient shown for the turbulent wind flow shown in Fig. 10.

The dynamic pressure on the reflector was then calculated according to the following equations:

$$U_m = \frac{U_{\text{gust}}}{1.6}, \tag{2}$$

$$U = U_m \left(\frac{H}{10} \right)^n, \tag{3}$$

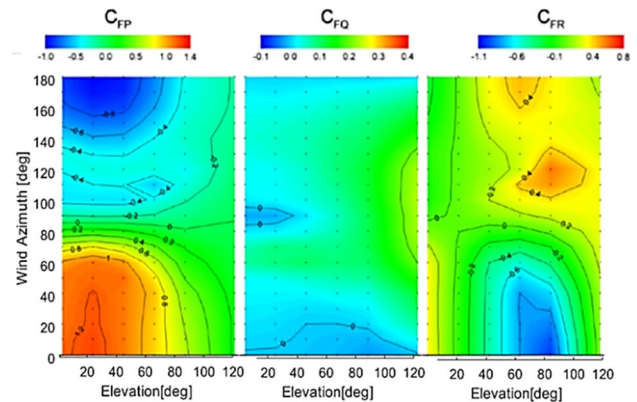


Fig. 9 Wind drag coefficient for the laminar flow [9]

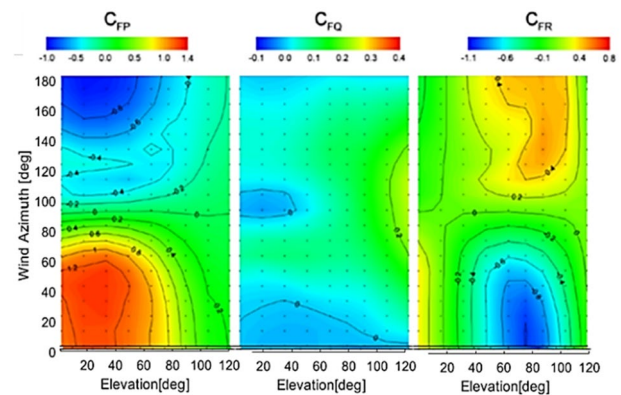


Fig. 10 Wind drag coefficient for the turbulent flow [9]

Table 4 Wind drag loads for the different operation conditions

Operation condition	Dynamic pressure	Load
Precise operation	19.43 Pa	43.7 N
Normal operation	39.65 Pa	89.2 N
Survival	1,675.00 Pa	3,768.0 N

Table 5 Panel requirements from the ngVLA global antenna parameters

Parameter	Requirement
Dimensions	1.5 m × 1.5 m
Surface accuracy	≤ 40 μm RMS
Material	Aluminum
Weight	≤ 20 kg /m ²
Normal Op Max deformation	≤ 10 μm RMS
Precision Op Max deformation	≤ 5 μm RMS
Gravity max deformation	≤ 30 μm RMS

$$Q = \frac{1}{2} \rho U^2 C_{FP}, \tag{4}$$

where U_m is the mean wind speed, U_{gust} is the maximum gust speed, H is the panel height, n is the power law exponent for the approaching wind (0.14 for open terrain), Q is the dynamic pressure, ρ is the air density, and C_{FP} is the wind drag coefficient. Calculating the corresponding load to each panel will multiply the dynamic pressure and panel area. The calculated loads for each operating condition are listed in Table 4.

A static structural FEA was performed on a panel reference model to determine the maximum deformation during operating conditions described in Table 5 and the maximum stress during survival conditions. The study covered the static structural analysis of a panel with the geometric characteristics described in Table 3 under the gravity and wind loads calculated in the preceding subsections. The study used the FEA software AnsysWorkbench 18.2 to perform the simulation.

Three operation conditions were evaluated for this study with different parameters. The first is called “precision operating conditions,” which defines the mean wind speed as 5 m/s with gusts of 7 m/s. The second, called “normal operation conditions,” defines the mean wind speed as 7 m/s with gusts of 10 m/s. The third is called “survival operating conditions,” where the mean wind speed is 50 m/s with gusts of 65 m/s. The first and second operation condition design criteria were constrained with a maximum deformation of 5 μm and 10 μm surface RMS, respectively. The third operation condition design criteria were constrained by the

Table 6 Panel FEA results with normal operation wind loads

Parameter	Value
Wind gust @ 10 m	10 m/s
φ angle	0 deg
Dynamic pressure	39.66 Pa
Boundary conditions	1 pad fixed, 3 pads only 4 DoF
Gravity	0 m/s ²
RMSE _{panel} deformation	7.6 μm

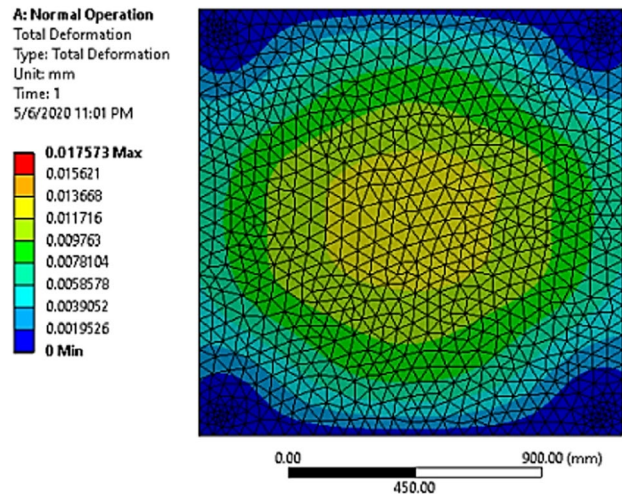


Fig. 11 Deformation plot for the reference panel model to the normal operation condition loads

Table 7 Panel FEA results with precise operation wind loads

Parameter	Value
Wind gust @ 10 m	7 m/s
φ angle	0 deg
Dynamic pressure	19.43 Pa
Boundary conditions	1 pad fixed, 3 pads only 4 DoF
Gravity	0 m/s ²
RMSE _{panel} deformation	3.7 μm

maximum allowed stress, such as the yield strength over a safety factor.

The first scenario is the wind drag for the normal operation condition. The boundary conditions included fixing all 6 DoFs on one pad and only 4 DoFs (R_x , R_y , R_z , and Z displacements) on the others. The φ angle is defined

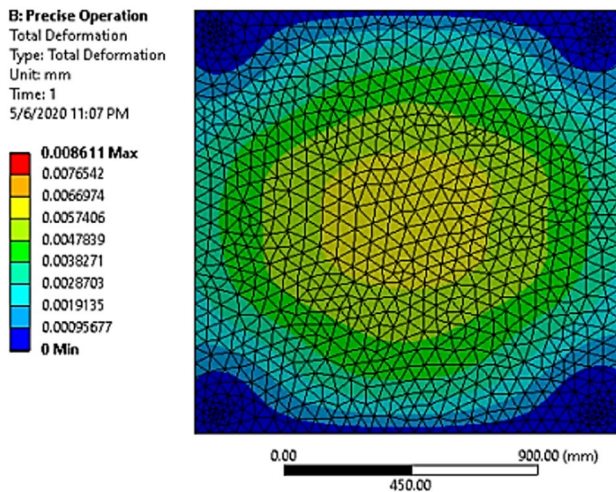


Fig. 12 Deformation plot for the panel reference model to the precision operation condition loads

between the panel normal vector and horizon. The results are summarized in Table 6 and depicted in Fig. 11.

The next scenario was the precise operation, where the wind gust was reduced to 7 m/s. The results are summarized in Table 7, and the FEA result is depicted in Fig. 12.

The simulation results show that the deformation for the three scenarios/operating conditions (only two shown) was below the requirements listed in Table 5. The precise operation load of 19.43 Pa caused by a wind with maximum gusts of 7 m/s resulted in a deformation of 3.7 μm RMS, which is below the required 5 μm . The normal operation conditions estimated a load of 39.65 Pa caused by a wind having maximum gusts of 10 m/s. For this scenario, the estimated deformation was 7.6 μm RMS, which is below the 10 μm required. Finally, the gravity condition (not shown) resulted in a deformation of 29.9 μm RMS, which is just below the 30 μm RMS requirement. The positions analyzed in the simulations refer to the worst-case scenario for the panels, and it is assumed that the rest of the panels will have deformation magnitudes below the values estimated for these scenarios. Nevertheless, the calculated scenarios show only isolated cases and no combination of loads as will occur in real operation conditions.

7 Conclusions

The adaptable thermoforming technology is primarily motivated to aid in the advancement of radio- and millimeter-wave telescope panel fabrication by developing a novel technology that has the potential to greatly improve the efficiency and required costs that are associated with the manufacturing process due to its efficient, repeatable, and

reusable nature when compared with current processes. The adaptable mold technology was introduced and summarized, specifically detailing the technology development process toward constructing and testing the adaptable mold, thermoformed panels, and a proposed panel structural design analyzed under realistic operational conditions and associated loads to provide a proof of concept for applying our technology toward real-world engineering applications. In addition, the springback calibration factor was determined by comparing the mold and panels' metrology data.

Acknowledgements This work was funded by the National Science Foundation (NSF) Award 2009384.

Declarations

Conflict of interest On behalf of all authors, the corresponding author states that there is no conflict of interest.

Open Access This article is licensed under a Creative Commons Attribution 4.0 International License, which permits use, sharing, adaptation, distribution and reproduction in any medium or format, as long as you give appropriate credit to the original author(s) and the source, provide a link to the Creative Commons licence, and indicate if changes were made. The images or other third party material in this article are included in the article's Creative Commons licence, unless indicated otherwise in a credit line to the material. If material is not included in the article's Creative Commons licence and your intended use is not permitted by statutory regulation or exceeds the permitted use, you will need to obtain permission directly from the copyright holder. To view a copy of this licence, visit <http://creativecommons.org/licenses/by/4.0/>.

References

1. Cheng J (2009) Fundamentals of radio telescopes. In: Cheng J (ed) The principles of astronomical telescope design. Springer, New York, NY, pp 339–376
2. Baars JWM, Kärcher HJ (2018) Evolution of the telescope. In: Baars JWM, Kärcher HJ (eds) Radio telescope reflectors: historical development of design and construction. Springer International Publishing, Cham, pp 9–30
3. Cheng J (2009) Millimeter and submillimeter wavelength telescopes. In: Cheng J (ed) The principles of astronomical telescope design, vol 360. Springer, New York, pp 443–499
4. Baars JWM, Kärcher HJ (2018) Emergence of millimetre-wavelength telescopes. In: Baars JWM, Kärcher HJ (eds) Radio telescope reflectors: historical development of design and construction. Springer International Publishing, Cham, pp 107–152
5. Davila-Peralta C et al. (2021) Electromagnetic thermoforming to manufacture reflective panels for radio telescopes and downlinks. In: 2021 IEEE aerospace conference (50100), Mar. 2021, pp. 1–15. doi: <https://doi.org/10.1109/AERO50100.2021.9438425>
6. Berkson J et al. Super depth resolution stereo matching based on fringe projection profilometry. Opt Express (submitted, under peer review)
7. Laurent H et al (2011) Mechanical behaviour and Springback study of an aluminium alloy in warm forming conditions. ISRN Mech Eng. <https://doi.org/10.5402/2011/381615>
8. Z. Hatfield et al. (2021) Adaptive aluminum thermoforming for precision millimeter wave telescope panels. In: OSA optical

design and fabrication (flat optics, freeform, IODC, OFT) (2021), paper OW2B.4, Jun. 2021, p. OW2B.4. doi: <https://doi.org/10.1364/OFT.2021.OW2B.4>

9. McAuliffe BR (2010) Wind tunnel investigations of symmetric- and offset-reflector radio telescope antennas for the square kilometre array (SKA): mean wind loads and surface pressures